Supplementary Materials

Decoupling ion/electron transport through laser-engineered vertical microchannels for high-loading solid-state lithium metal batteries

Yongbiao Mu[1,2,3], Chengjun Xu[4], Maokun Li[1], Chaozhu Huang[1,2], Zigeng Wu[1], Lin Yang[1,2], Yitian Feng[1,2], Zetao Chen[1,2], Hanshun Lai[1,2], Zhiyu Zou[1,2], Hengyuan Hu[1,2], Guobin Zhang[5], Meisheng Han[1,2,*], Liang An[3,*], Lin Zeng[1,2,*]

[1]Shenzhen Key Laboratory of Advanced Energy Storage, Department of Mechanical and Energy Engineering, Southern University of Science and Technology, Shenzhen 518055, Guangdong, China.
[2]SUSTech Energy Institute for Carbon Neutrality, Southern University of Science and Technology, Shenzhen 518055, Guangdong, China.
[3]Department of Mechanical Engineering, The Hong Kong Polytechnic University, Kowloon 999077, Hong Kong, China.
[4]School of Energy Science and Engineering, Nanjing Tech University, Nanjing 210000, Jiangsu, China.
[5]College of New Materials and New Energies, Shenzhen Technology University, Shenzhen 518118, Guangdong, China.

Correspondence to: Dr. Meisheng Han, Department of Mechanical and Energy Engineering, Southern University of Science and Technology, No. 1088 Xueyuan Avenue, Nanshan District, Shenzhen 518055, Guangdong, China. E-mail: hanms@sustech.edu.cn; Prof. Liang An, Department of Mechanical Engineering, The Hong Kong Polytechnic University, Hung Hom, Kowloon 999077, Hong Kong, China. E-mail: liang.an@polyu.edu.hk; Prof. Lin Zeng, Department of Mechanical and Energy Engineering, Southern University of Science and Technology, No. 1088 Xueyuan Avenue, Nanshan District, Shenzhen 518055, Guangdong, China. E-mail: zengl3@sustech.edu.cn

COMSOL Simulation Details

General setup

The finite element analysis simulations are performed with the COMSOL Multiphysics software. Simulation analysis of ion concentration was conducted for two models:

1. **Comparison sample**: Electrolyte as an independent membrane attached to the surface of a thick electrode.
2. **Experimental sample**: Laser-drilled + electrolyte-cast integrated electrode.

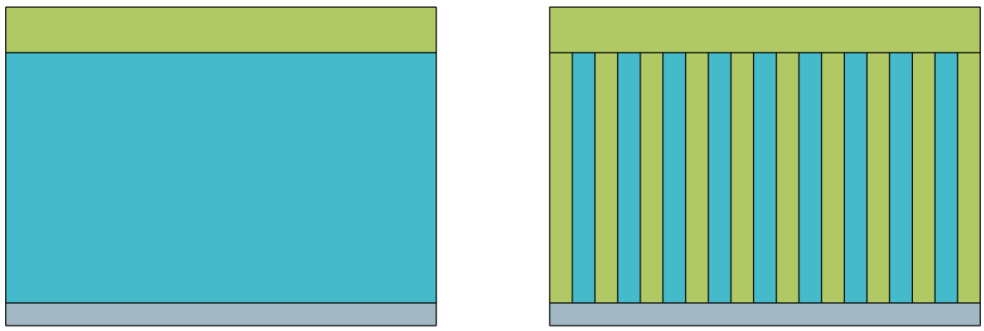

By simulating the ion concentration distribution within the two models, the study aims to reveal the influence of different electrolyte–electrode composite configurations on ion concentration distribution. The simulation consists of three parts: 1. Current collector; 2. Cathode material; 3. Electrolyte. Ions flow from within the cathode material and exit through the interface between the electrode and the electrolyte.

Theoratical mothod

1. Transport of Diluted Species (in the electrolyte and electrode domains)

The mass balance for a diluted species i is governed by the diffusion-convection equation. Assuming no convection in the solid domains, it reduces to Fick's second law:

$$\frac{\partial c_i}{\partial t}+\nabla\cdot\mathbf{J}_i=R_i$$

Where:

c_i= Concentration of species i [mol/m³]

t= Time [s]

$\mathbf{J}_i$= Flux vector of species i [mol/(m²·s)]

R_i= Reaction rate source/sink term [mol/(m³·s)]

The flux $\mathbf{J}_i$ is defined by Fick's first law of diffusion (and optionally migration if an electric field is considered):

$$\mathbf{J}_i = -D_i \nabla c_i - z_i u_{m,i} F c_i \nabla \phi_l$$

Where:

D_i = Diffusion coefficient of species i [m²/s]

z_i = Charge number of the ionic species (valence)

$u_{m,i}$ = Ionic mobility [s·mol/kg]

F = Faraday's constant [C/mol]

ϕ_l = Electrolyte potential [V]

2. Electrode/Electrolyte Interface Condition

At the interface between the electrode and the electrolyte, the flux is determined by the electrochemical reaction rate, typically described by the Butler-Volmer equation:

$$\mathbf{n} \cdot \mathbf{J}_i = \frac{i_{loc}}{nF}$$

Where:

$\mathbf{n}$ = Normal vector pointing outward from the boundary

$\mathbf{J}_i$ = Ionic flux normal to the interface [mol/(m²·s)]

i_{loc} = Local current density [A/m²]

n = Number of electrons transferred in the reaction

These equations form the core of ion transport and electrochemical kinetics in the COMSOL model.

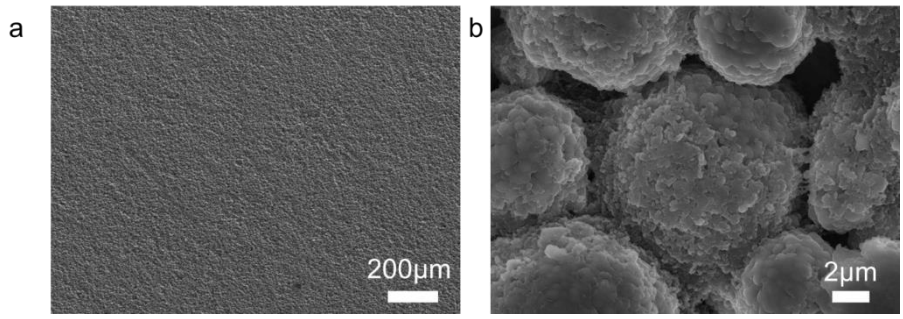

Figure S1. (a) Low-magnification and (b) high-magnification SEM images of a commercial NCM cathode (20 mg cm^{-2}).

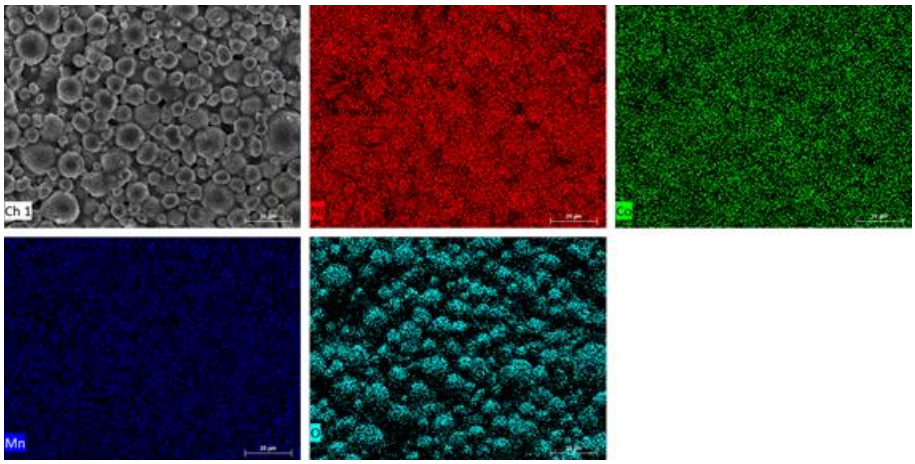

Figure S2. EDS-mapping images of a commercial thick NCM cathode including Ni, Co，Mn and O elements.

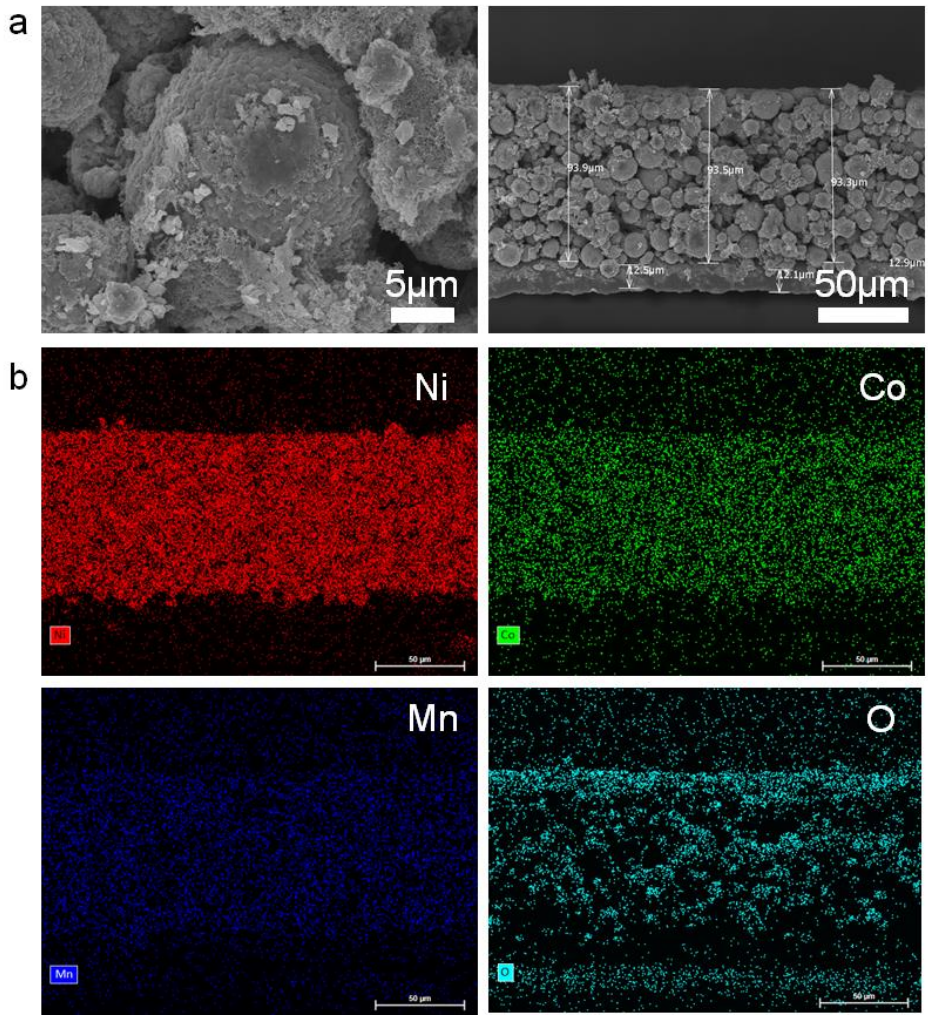

Figure S3. (a) SEM images of a commercial thick NCM cathode from cross-setional view, and (b) including Ni, Co, Mn and O elements.

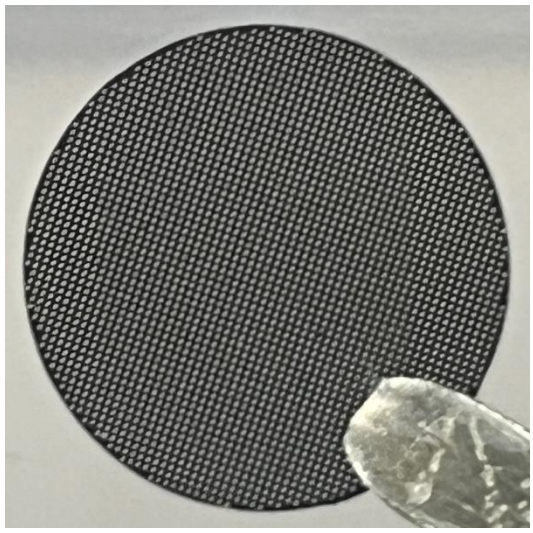

Figure S4. Optical image of the laser-structured thick NCM811 electrode.

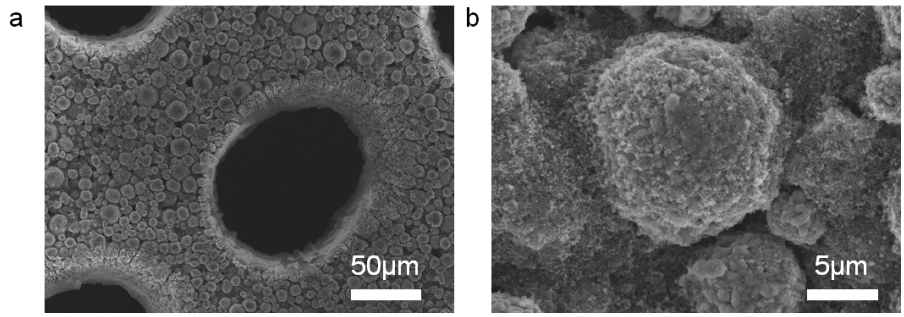

Figure S5. (a) Low-magnification and (b) high-magnification SEM images of the laser-structured NCM cathode.

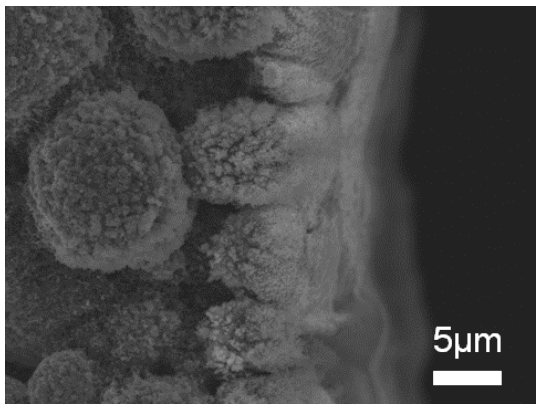

Figure S6. High-magnification SEM images of the laser-structured NCM cathode near the hole.

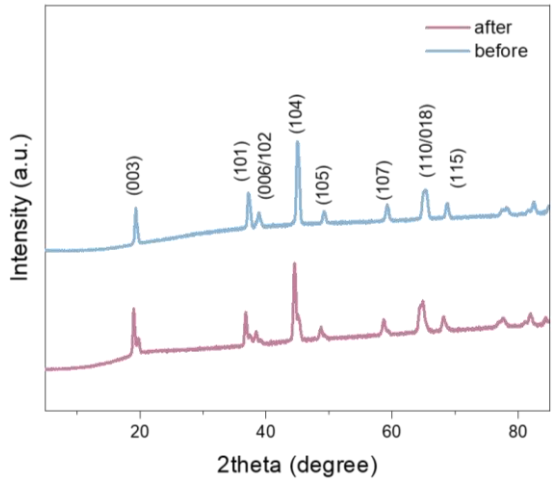

Figure S7. XRD patterns of the pristine cathode and the laser-patterned cathode.

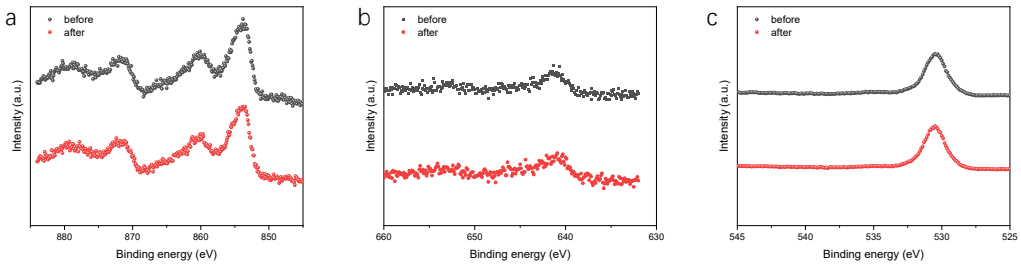

Figure S8. XPS analysis of (a) Ni 2p, (b) Mn 2p, and (c) O 1s for the pristine cathode and the laser-patterned cathode.

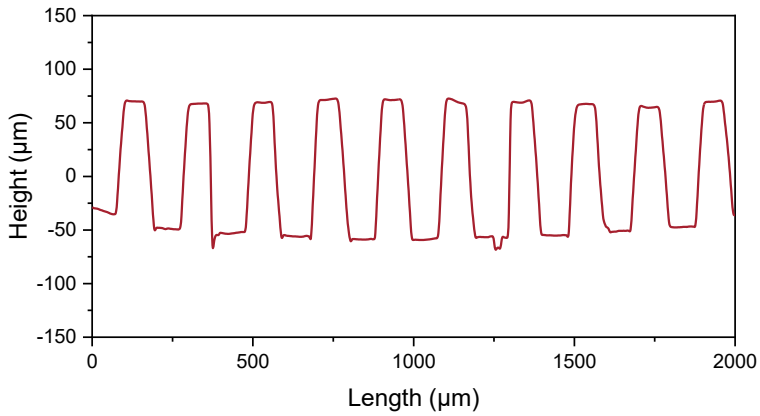

Figure S9. Surface profile of NCM electrode pore structure obtained from confocal microscopy.

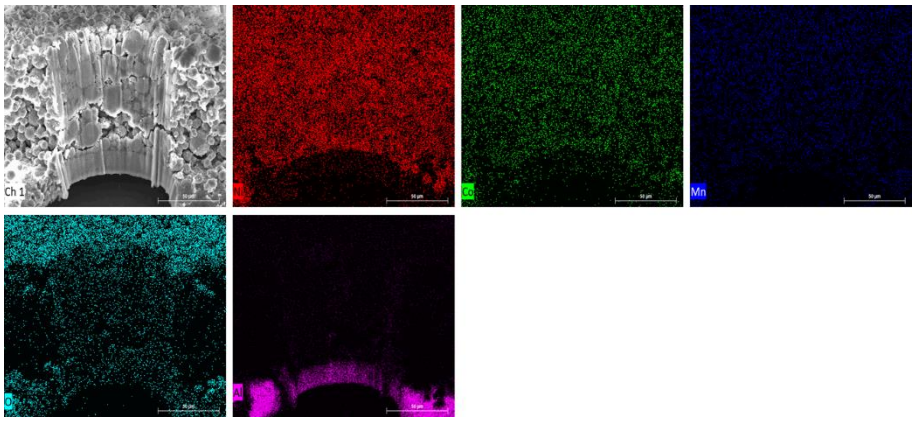

Figure S10. EDS-mapping images of a laser-sructured NCM cathode including Ni, Co， Mn, O, and Al elements.

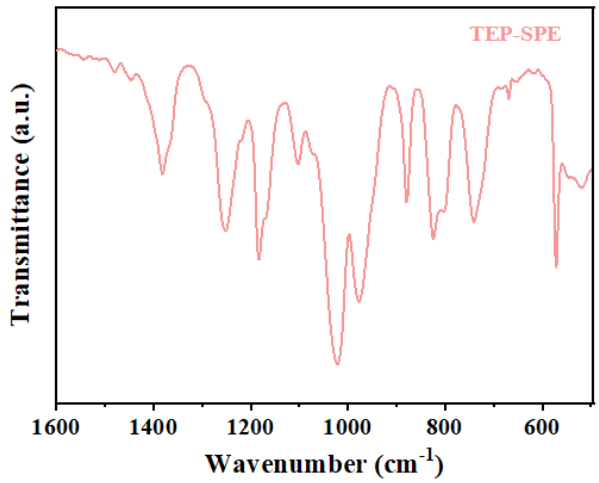

Figure S11. FTIR spectra of solid polymer electrolyte.

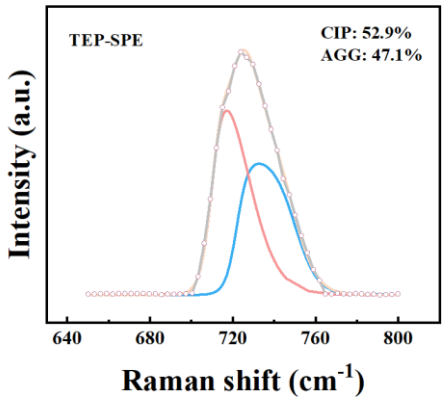

Figure S12. Raman spectra of solid polymer electrolyte.

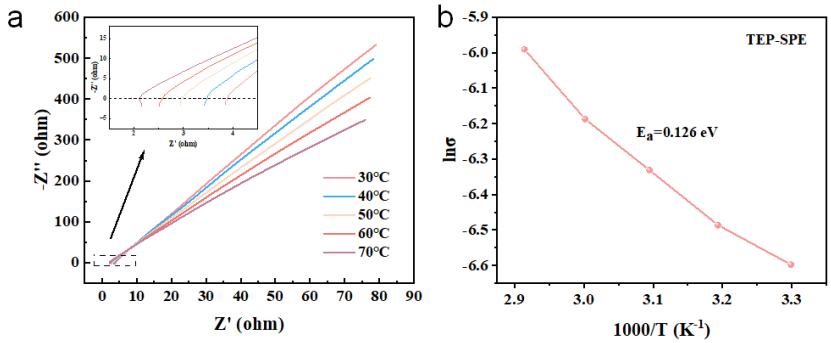

Figure S13. (a) EIS spectra of solid polymer electrolyte under different temperature from 30 to 70 ℃, and (b) activation energy profile of the Li-ion diffusion process.

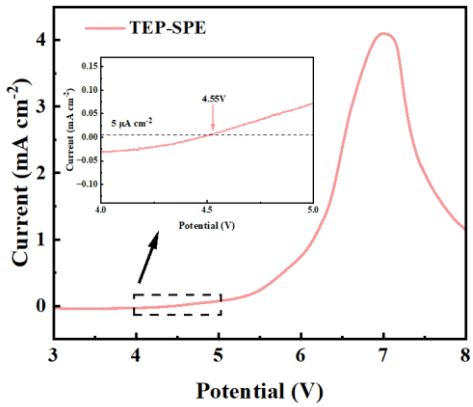

Figure S14. LSV curve of the solid polymer electrolyte.

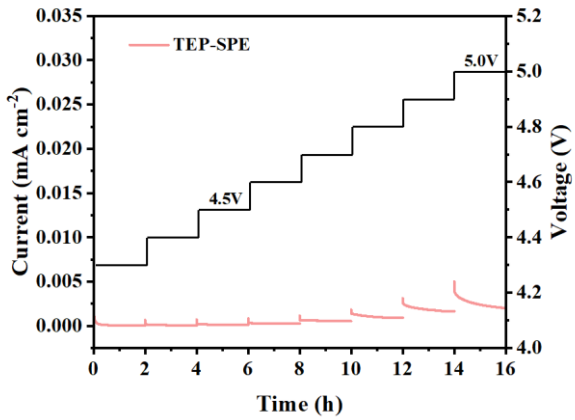

Figure S15. Electrochemical floating test of solid polymer electrolyte.

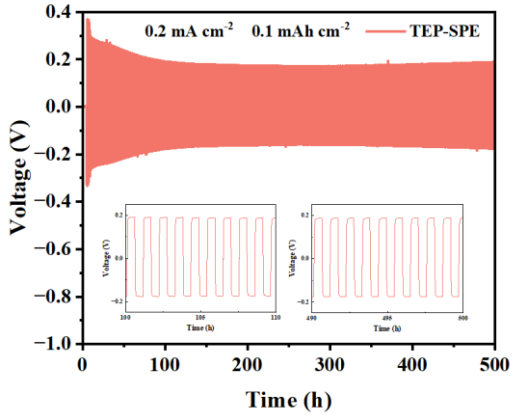

Figure S16. Cycle performance of Li||SPE||Li cell under 0.2 mA cm^{-2} and 0.1 mAh cm^{-2}.

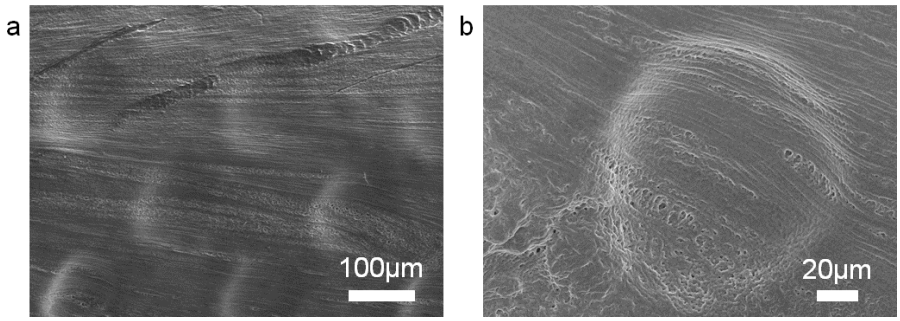

Figure S17. (a) Low-magnification, and (b) high-magnification SEM images of the SPE-infiltrated NCM electrode with laser-structured pore arrays.

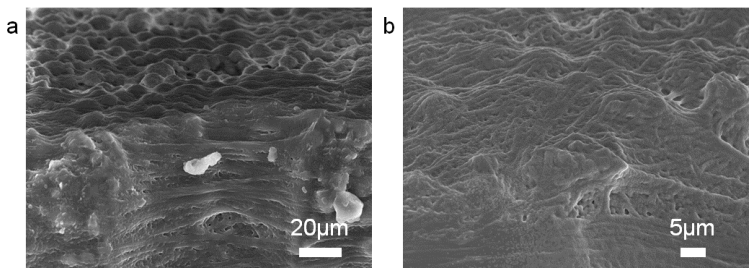

Figure S18. Cross-sectional SEM images of the SPE-infiltrated NCM electrode of (a) low-magnification, and (b) high-magnification.

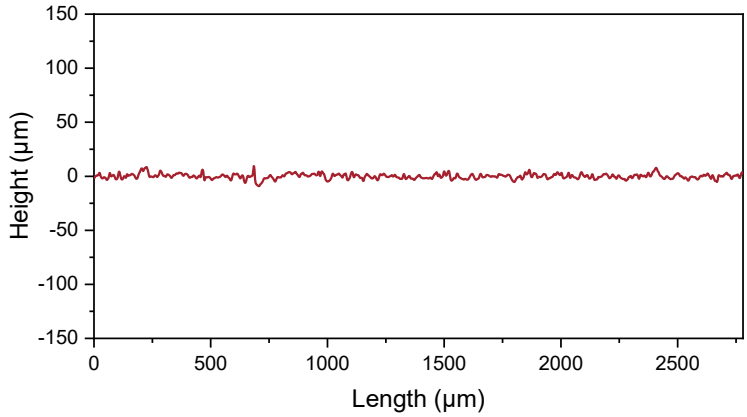

Figure S19. Surface profile of SPE-infiltrated NCM electrode obtained from confocal microscopy.

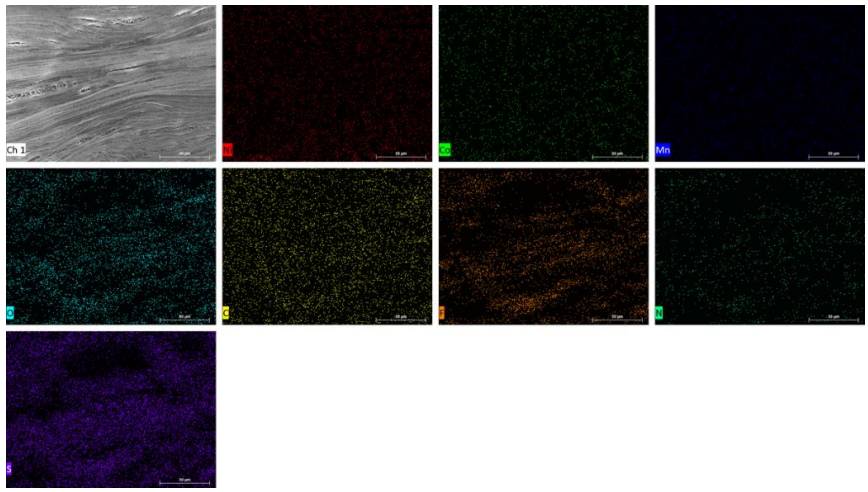

Figure S20. EDS-mapping images of a SPE-infiltrated NCM electrode including Ni, Co, Mn, O, C, F, N, and S elements.

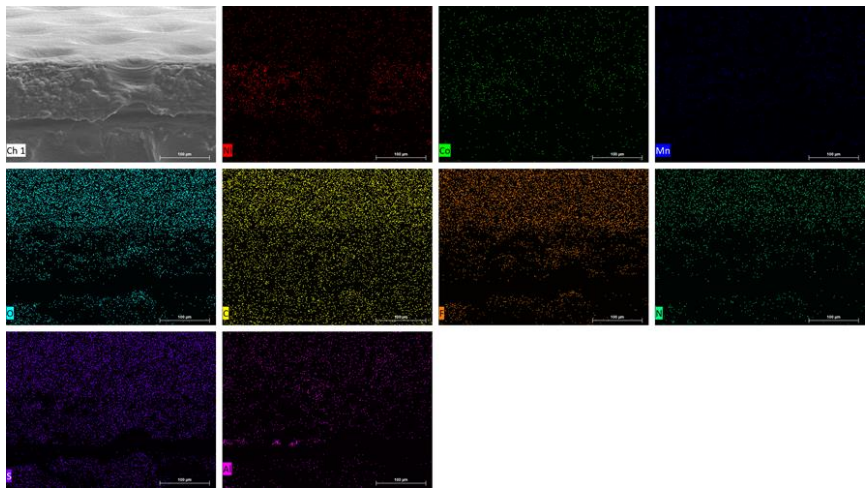

Figure S21.EDS-mapping images of a SPE-infiltrated NCM electrode from cross-sectional view including Ni, Co, Mn, O, C, F, N, S and Al elements.

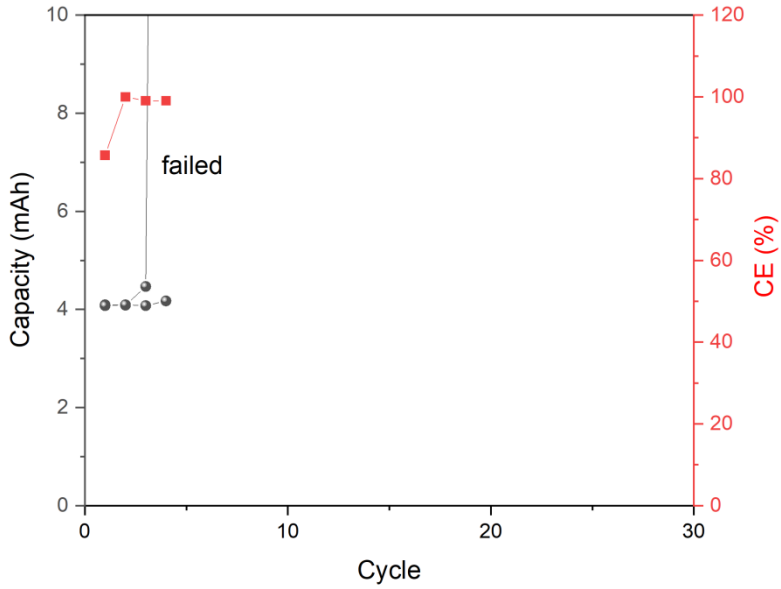

Figure S22. Rate performance of Li||NCM811 cell with conventional SPE under 2.8~4.3 V at 0.2C.

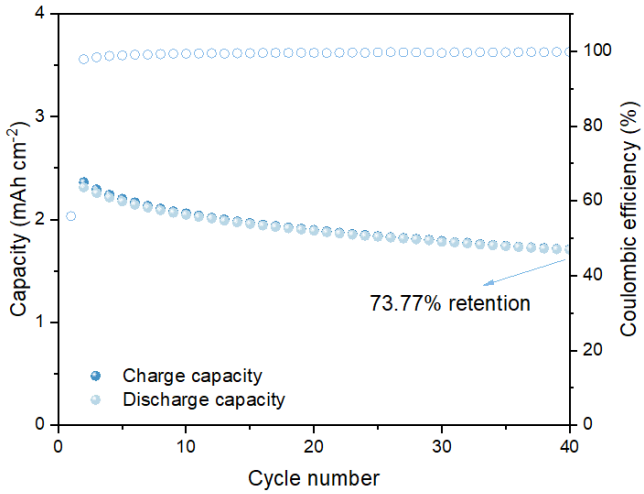

Figure S23. Cycle performance of Li||NCM811 cell with conventional SPE under 2.8~4.3 V at 0.2C.

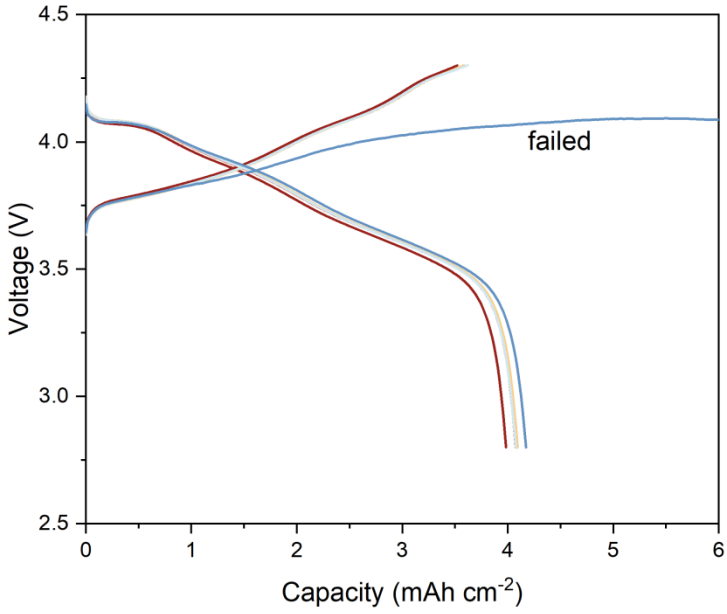

Figure S24. GCD curves of Li||NCM811 cell with conventional SPE under 2.8~4.3 V at 0.2C.

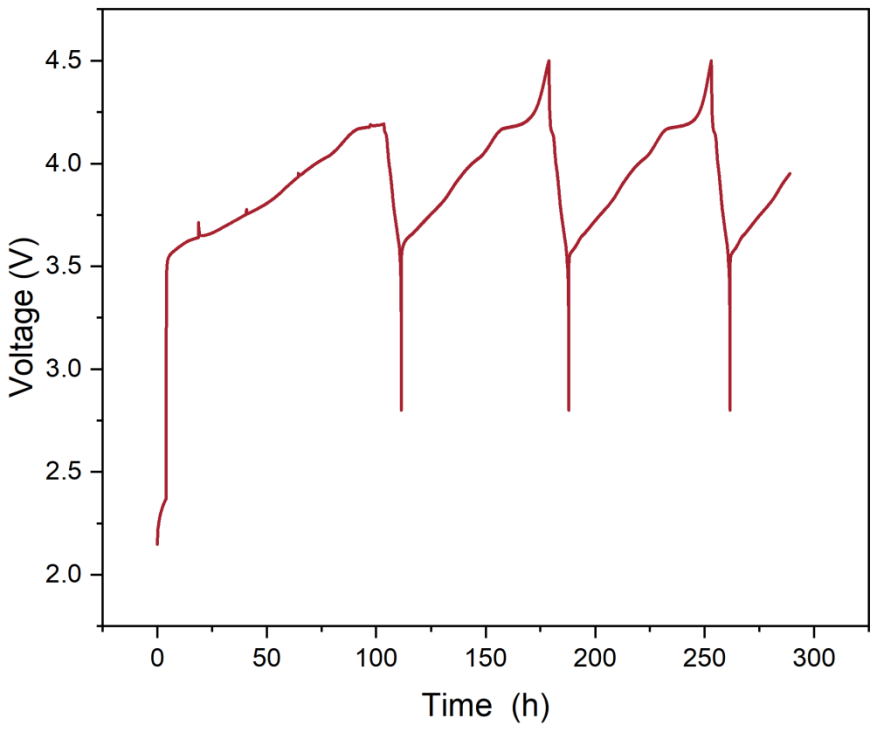

Figure S25. Cycle performance of Li||NCM811 cell with conventional SPE under 2.8~4.5 V at 0.2C.

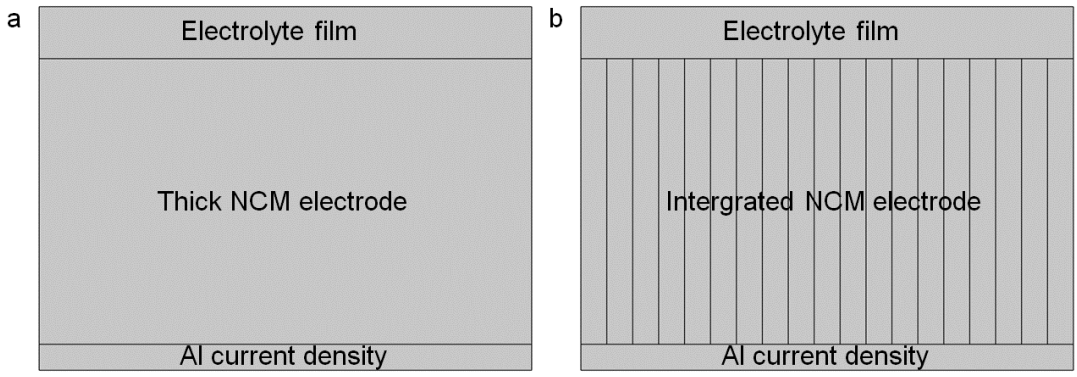

Figure S26. Two different electrolyte–electrode composite configurations: (a) conventional electrode, and (b) intergrated 3D NCM electrode.

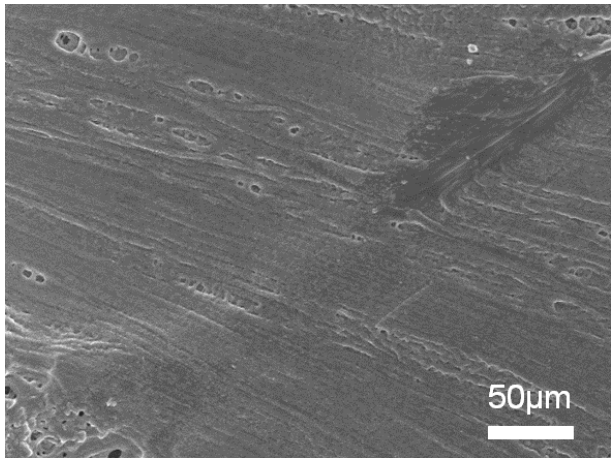

Figure S27. SEM image of the cycled SPE-infiltrated NCM electrode.

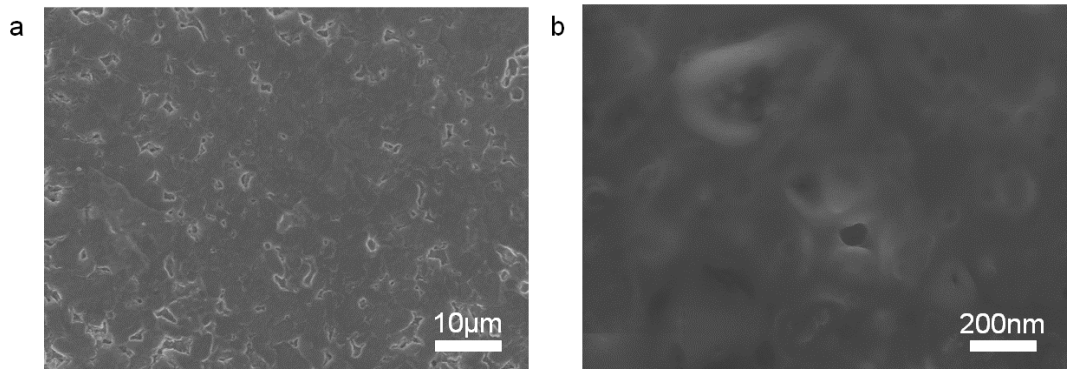

Figure S28. SEM images of the cycled Li metal anode of (a) low magnification and (b) high magnification.

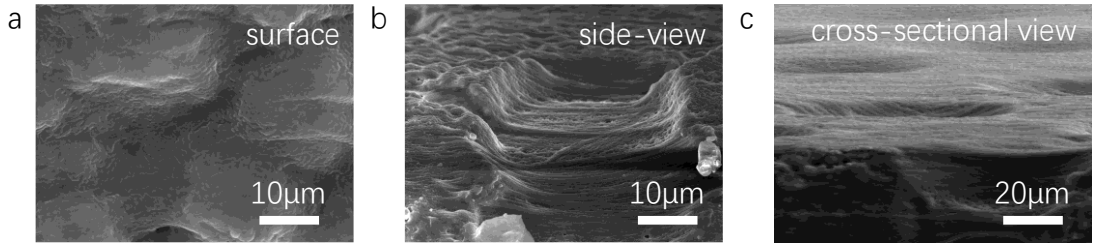

Figure S29. SEM images of the cycled NCM811 cathode from different views (a-c).

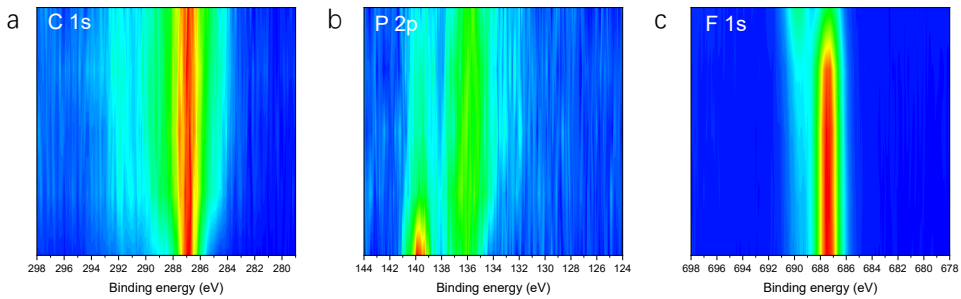

Figure S30. XPS depth-profiling analysis of the cycled composite SE/NCM811 cathode: (a) C 1s, (b) P 2p, and (c) F 1s.

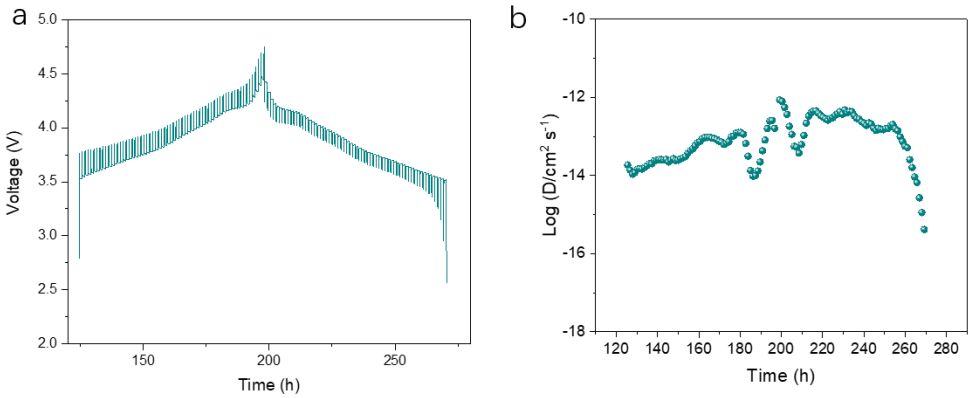

Figure S31. (a) GITT profiles of the conventional NCM811 electrode. (b) Li^+ diffusion coefficients of the conventional NCM811 electrode as a function of the charge/discharge state.

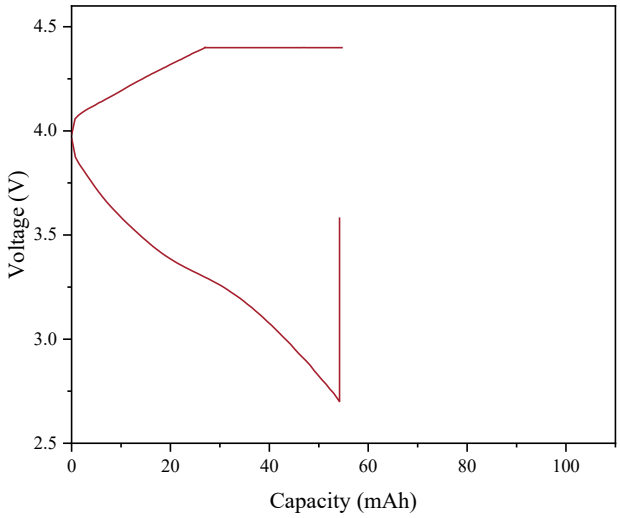

Figure S32. Charge-discharge curves of pouch cells using the conventional NCM811 cathode.

Table S1. Summary table of mass loadings of active material for different types of NCM811 electrodes.

Electrodes	Mass loading of total electrode	Mass loading of current collector	Mass loading of total electrode
Bare NCM811 electrode	21.4 mg	5 mg (12mm)	15.74 mg
NCM811 electrode before patterned	28.5 mg	5 mg (12mm)	22.56 mg
NCM811 electrode after patterned	21.9 mg	4.2 mg (12mm)	16.60 mg

Table S2. Summary of the performance of this NCM cathode with other reported ploymer solid-state cathodes from recent literature.

Cathodes	Electrolytes	Voltage windows (V)	Mass loading (mg cm^{-2})	Rates (C)	Temperture (℃)	Cycle performance	Refs.
NCM622	AlF 3-Poly-DOL	3.0-4.2	3.0 mAh cm^{-2}	0.1C	RT	60; 80%	1
NCM811	PVDF-PAN	3.3-4.5	3.5	0.1C	RT	200; 68.2%	2
NCM811	C@LATP NW/PVDF	2.8-4.3	15	0.1C	RT	50; 85%	3
NCM811	AIP	2.7-4.3	5	1C	30	200; 93.2%	4
NCM811	SIP-derived SPE	2.7-4.3	5	0.5C	65	120;＞95%	5
NCM712	TC-GPEs	3.0–4.3	7.7	1C	30	150; 90.9%	6
NCM811	**TD/PVDF**	**2.7–4.5**	**14.7**	**0.2C**	**30**	**100; 95.8%**	**This work**

References

1. Zhao, C.-Z., et al., Advanced Materials (2020) 32 (12), 1905629
2. Jiang, H., et al., Journal of Energy Chemistry (2023) 78, 277
3. Liu, Y., et al., Energy & Environmental Science (2024) 17 (1), 344
4. Yang, J., et al., Advanced Energy Materials (2021) 11 (39), 2101956
5. Chen, Y., et al., Advanced Materials (2023) 35 (18), 2300982
6. Choi, M. S., et al., Angewandte Chemie (2025) 137 (17), e202424568